

## Front dynamics in the Harper model

Gergő Roósz 

Wigner Research Center for Physics, P.O. Box 49, 1525 Budapest, Hungary

 (Received 11 June 2023; revised 9 November 2023; accepted 11 January 2024; published 14 February 2024)

The front dynamics in the Harper (or Aubry-André) model (which has a localization transition) is investigated using two different settings: the particle number front, where the system is at zero temperature and, initially, the particle numbers differ on the two sides, and the temperature front, where the two sides have different temperatures initially. The two differently prepared half systems are connected suddenly, and the following dynamics is investigated. In the extended phase, the dynamics is ballistic, similar to the dynamics of a pure system. At the critical point, one finds a power-law time dependence of the particle number and the entanglement entropy of the zero-temperature setting. In the localized phases, the observables oscillate around an average value, which is independent of the system size. The particle number front shapes have been investigated at the zero-temperature setting: In the extended phase they scale together exactly as in the homogeneous XX chain; however, at the critical point the scaling relation contains a power ( $t^{0.55}$ ) of time. The mutual information between neighboring intervals at the front has been calculated, and it is proportional to the logarithm of the interval length and also to the logarithm of time in the extended phase and at the critical point. The prefactors of the time and size dependence are equal for the zero-temperature process but differ for the finite-temperature front.

DOI: [10.1103/PhysRevB.109.064204](https://doi.org/10.1103/PhysRevB.109.064204)

### I. INTRODUCTION

When two systems prepared in states with different properties (e.g., particle number and temperature) are suddenly connected, a nontrivial dynamical process starts, where the disturbed region (the so-called front) broadens with time starting from the point of connection; this process is usually referred to as front dynamics.

From analytical results involving the XX chain [1–4], one learns that as the disturbed region broadens with time, its shape varies. In an infinite system, the front broadens without limit, and in a finite system the front is reflected from the ends. For example, the magnetization in the XX chain when the starting state is a magnetic kink evolves according to a simple scaling function  $m(n, t) = \Phi(n/t)$  ( $n$  is the place coordinate, and  $t$  is time). This means the ballistic broadening of the front.

In one of the first studies of dynamical steady states [5,6] the authors proved that the steady state in the XX chain can be prepared as a ground state of the Hamiltonian with current generators added.

A later study [7] investigated the XX chain after connecting two half-infinite segments with different temperatures (I call it here the temperature front). The authors of Ref. [7] investigated the mutual information between two neighboring intervals and both intervals inside the front region when the steady state was already built up. It has been found that the mutual information grows with the log of the interval size,  $I \sim \ln l$ , and (between the two half-infinite chains) with the log of time,  $I \sim \ln t$ ; in addition, the two prefactors are equal. There are a series of further results involving the details of the XX front dynamics: The statistics of particle numbers at the front has been calculated [8], there are analytical results regarding the magnetization profile scaling in an external magnetic field [9], the spin current fluctuations have been obtained [10], and the entanglement Hamiltonian has been obtained using

bosonization [11]. In the transverse Ising model and in the XY model [3,12–19], the general scaling of the front is similar to the scaling of the front of the XX model, with several minor differences.

Several studies have investigated the XXZ chain [20–30]. From these results involving the XXZ chain, I would like to highlight that although the dynamics is ballistic (as in XX or Ising chains) for most initial states, there are special initial states with subdiffusive behavior [23] and a region has been found where the transport stops [30]. So the dynamics is strongly dependent on the initial state, which is an important difference compared with quench dynamics, where the effect of the initial state is small [31].

Talking about methods, there are results in exactly solvable models, for example, a canonical transformation [32] after a Jordan-Wigner transformation [33] in the XX, XY, and Ising chains, and using other analytical solutions in the harmonic chain [34] or the sine-Gordon [35] model. When the analytical solution is not known, one may approximate the original model with a solvable one (in one dimension it is often a Luttinger liquid approximation obtained by bosonization [11,22,24,27]) or follow the time evolution with a numerical method, such as time-evolving block decimation [25,26] or the time-dependent density matrix renormalization group (DMRG) [28,30].

On the other hand, one may concentrate on the physical impact of local disturbances rather than strictly following the unitary dynamics. Local disturbances in one-dimensional quantum systems create an effect, which spreads according to a light cone. This physical observation led to the invention of the quasiclassical description of the dynamics of one-dimensional noninteracting quantum systems, first applied to the description of global quenches [36–39]. This method and its generalization to Bethe ansatz integrable systems has been

successfully applied to the front dynamics [40–54]. Depending on the model, precise approximations or even exact results have been obtained using semiclassical dynamics and generalized hydrodynamics.

For noninteracting aperiodic and disordered models, numerical results for global sudden quenches have been qualitatively interpreted assuming that signals spread with anomalous diffusion (aperiodic systems) or with the logarithm of time (in disordered systems) [55–57].

The goal of the present study is to investigate the front dynamics at a localization transition and answer the following question: If the shapes of the fronts are different at the transition point, what is the behavior of the mutual information in the front region?

The rest of the paper is organized as follows. In Sec. II the model is defined, and its equilibrium properties are presented. In Sec. III the local particle numbers, entanglement entropy, and mutual information are defined. In Sec. IV the numerical results are presented, and in the Conclusions, I discuss the results. In the Appendix, technical details of the time evolution are given.

## II. MODEL

The Harper model is defined as follows:

$$H = -\frac{1}{2} \sum_{l=1}^{L-1} c_l^\dagger c_{l+1} + c_{l+1}^\dagger c_l + h \sum_{l=1}^L \cos(2\pi\kappa l) c_l^\dagger c_l, \quad (1)$$

where  $c_l$  and  $c_l^\dagger$  are the fermionic annihilation and creation operators for  $l = 1 \dots L$ ,  $L$  is the length of the systems,  $h$  is an external parameter (the amplitude of the inhomogeneity), and  $\kappa = (1 + \sqrt{5})/2$ . There is a localization transition in the model [58]: For  $h < 1$ , every eigenstate is delocalized, free-wave-like; for  $h > 1$ , every eigenstate is localized. The localization length for  $h > 1$  is given by [58,59]

$$l_{\text{loc}} = \frac{1}{\ln h}. \quad (2)$$

The system is self-dual to the critical point: A (modified) Fourier transform maps the  $H$  operator with  $h$  to a similar operator with  $1/h$  [31,58–60]. The localization transition occurs for every irrational  $\kappa$ ; the localization length [Eq. (2)] and the self-duality are also not sensitive to  $\kappa$ , until  $\kappa$  is irrational [61]. However, the details of the transition are sensitive to the  $\kappa$  value. It has been shown with renormalization group studies [62] and numerical calculations [63] that the  $z$  critical exponent depends on  $\kappa$ .

The spectrum is continuous in the extended phase, fractal at the critical point, and pure point spectra in the localized phase [64]. The one-particle eigenstates are multifractals at the critical point [65,66]. In the ground state at half filling [67] the entanglement entropy of an interval of length  $l$  scales as

$$S = 0.33 \ln l; \quad (3)$$

so the scaling is identical to that of the homogeneous XX chain ( $c_{\text{eff}} = 1$ ). At the critical point of the system, the

effective central charge changes [67]:

$$S = 0.21 \ln l. \quad (4)$$

This corresponds to  $c_{\text{eff}} \approx 0.78$ . In the localized phase the entanglement entropy saturates to a constant value in the  $L \rightarrow \infty, l \rightarrow \infty, l/L = \text{const}$  limit. This entropy depends on the localization length as

$$S_{\text{sat}} \sim \frac{c_{\text{eff}}}{3} \ln(l_{\text{loc}}). \quad (5)$$

The scaling of the logarithmic negativity follows the same effective central charges [67].

There are gaps in the spectrum of the Aubry-André model, both in the extended phase and at the critical points [58,68]. If one chooses the chemical potential (Fermi surface) at the location of one of these gaps, the system becomes noncritical (gapped), and the entanglement entropy follows the area law, which in one dimension means it remains constant [68]. In this paper, zero chemical potential has been used during the time evolution.

After a quantum quench (sudden change in  $h$ ) the dynamics depends mainly on the after-quench Hamiltonian [31]. If the after-quench Hamiltonian is in the extended phase, the dynamics resemble the dynamics of a homogeneous XX chain, and the entanglement entropy grows linearly in time,  $S \sim t$  [31]. At the critical point, the entanglement entropy grows as a power function of time,  $S \sim t^\sigma$ , and in the localized phase it remains bounded.

The model has been realized in an optical lattice with cold atoms [69–72], and a steplike initial condition of the occupation number has also been realized in cold-atom experiments [73]; so our zero-temperature particle number protocol might be possible to realize in these experiments.

## III. QUANTITIES OF INTEREST

I divide the system into two halves,  $A$  and  $B$ , where  $A$  contains the first  $[L/2]$  sites (where  $[\cdot]$  is the lower integer part) and  $B$  contains the rest of the system. The two halves are not connected for  $t < 0$  and are prepared in states with different physical parameters. At  $t = 0$  the two halves of the system are connected, and a nontrivial time evolution starts.

For the zero-temperature protocol, the particle number is different at  $t = 0$  in the two halves of the system, the  $A$  subsystem is empty, and the  $B$  subsystem is half filled.

In this case the system at  $t = 0$  is in a pure state  $|\psi_0\rangle$ , and the dynamics is given by the Schrödinger equation  $i \frac{\partial}{\partial t} |\psi(t)\rangle = H |\psi(t)\rangle$ .

For the finite-temperature protocol, at  $t = 0$  the  $A$  subsystem is at thermal equilibrium at temperature  $T_A$ , the  $B$  subsystem is at thermal equilibrium at temperature  $T_B \neq T_A$ , and the two halves are not connected. We connect  $A$  and  $B$  at  $t = 0$ , and the dynamics for  $t > 0$  is governed by the Hamiltonian equation (1). In our model, the couplings to the heat reservoirs which have created the initial thermal equilibrium (at two different temperatures) of the two halves are not present, and the dynamics is given by the Schrödinger equation. This corresponds (in experiments) to short time scales compared with the thermal equilibration timescale.

In this second protocol, the left and right subsystems are prepared in the

$$\rho_A = \frac{1}{Z_A} \exp[-\beta_A H_A], \quad (6)$$

$$\rho_B = \frac{1}{Z_B} \exp[-\beta_B H_B] \quad (7)$$

states, and the whole system is prepared in the

$$\rho = \rho_A \otimes \rho_B \quad (8)$$

state. For  $t > 0$  the dynamics is given by the equation  $i \frac{\partial}{\partial t} \rho(t) = [H, \rho]$ . Technically, I follow the time evolution of the operators in the Heisenberg picture; so the dynamics of the two protocols are the same, and only the initial state differs.

I investigate (for both protocols) the time evolution of the particle numbers in the two sectors ( $N_A$  and  $N_B$ ), as well as, for the zero-temperature protocol, the entanglement entropy of the two halves and, for the finite-temperature protocol, the mutual information between the two halves. For the zero-temperature protocol, I also investigate the finite-size scaling of the mutual information in the dynamical steady state [34]. This means that the mutual information is calculated between two intervals (of length  $l$ ) at the border between the two subsystems for interval lengths shorter than the half-system size for a given time  $t > 0$ . In this setting, one interval is from the  $(L/2 - l)$ th site to the  $(L/2)$ th site, and the other interval is from the  $(L/2 + 1)$ th site to the  $(L/2 + l)$ th site.

Let us take a closer look at the aforementioned quantities. The particle numbers are defined as the expectation values of the particle number operators

$$\hat{N}_A = \sum_{l \in A} c_l^\dagger c_l, \quad (9)$$

$$\hat{N}_B = \sum_{l \in B} c_l^\dagger c_l, \quad (10)$$

and  $N_A = \langle \hat{N}_A \rangle$  and  $N_B = \langle \hat{N}_B \rangle$ .

To define the mutual information and the entanglement entropy [74], one defines the reduced density matrices of the  $A$  and  $B$  subsystems. The density matrix of the whole system is  $\rho(t)$ ; this includes the special case of the pure state  $|\psi(t)\rangle$  as a projector  $\rho_{\text{pure}}(t) = |\psi(t)\rangle\langle\psi(t)|$ . The reduced density matrices are

$$\rho_A = \text{Tr}_B \rho, \quad (11)$$

$$\rho_B = \text{Tr}_A \rho. \quad (12)$$

Now, one defines three entropies: the entropy of the whole system and the entropies of the reduced density matrices.

$$S = -\text{Tr} \rho \ln \rho, \quad (13)$$

$$S_A = -\text{Tr}_A \rho_A \ln \rho_A, \quad (14)$$

$$S_B = -\text{Tr}_B \rho_B \ln \rho_B \quad (15)$$

for pure states  $S = 0$  and  $S_A = S_B$ . In this case the last two quantities are the entanglement entropy:

$$S_{\text{entangle}} = S_A = S_B. \quad (16)$$

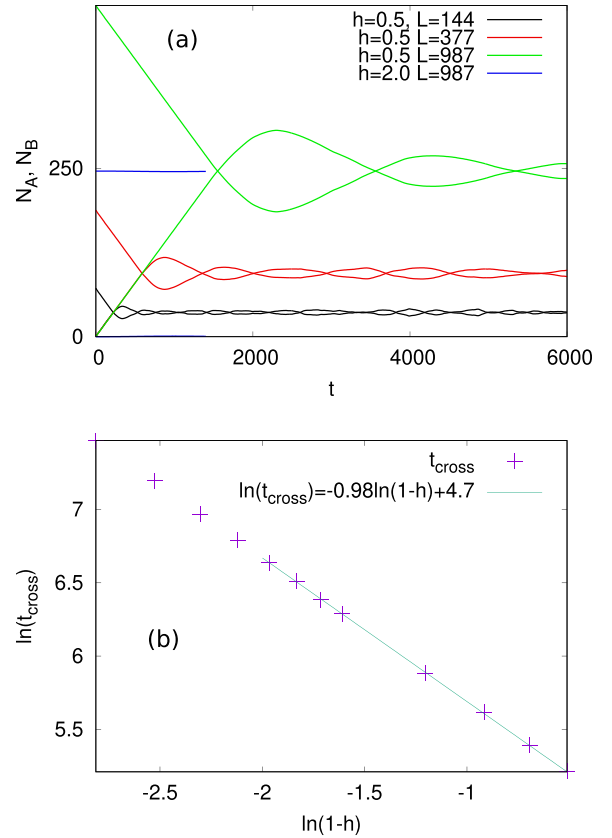


FIG. 1. (a) Typical behavior of the particle numbers of the two subsystems in the zero-temperature protocol. The colors denote the different quench parameters ( $h$  and  $L$ ). The particle numbers  $N_A$  and  $N_B$  from the same process are denoted by curves of the same color; one grows initially, and its pair decreases initially. (b) The logarithm of first crossing times of the particle numbers, as a function of  $\ln(1 - h)$ , for  $L = 144$ .

For nonpure states, the entropies of the two reduced density matrices are different ( $S_A \neq S_B$ ). In this case, one can quantify the total correlations between the two subsystems using the mutual information, which is defined as follows [75]:

$$I = S_A + S_B - S. \quad (17)$$

#### IV. RESULTS

In this section, numerical results are presented. The typical behavior of the particle number after this quench is shown in Fig. 1(a); in this figure there are data about quenches in the extended phase (at  $h = 0.5$ ) with three different system sizes ( $L = 144, 377, 987$ ), and there is one quench to the localized phase ( $h = 2.0$ ). One can see that in the localized phase the dynamics “froze” and the expectation value of  $N_A$  and  $N_B$  remains close to the initial values. In the extended phase, the particle numbers change. For short times the particle number of the initially empty subsystem grows linearly, and the particle number of the initially half-filled subsystem decreases linearly with the same slope. At an intermediate time, the particle numbers of the two halves are equal, the curves cross each other, oscillating behavior starts, with decreasing oscillation amplitude, and for a very long time the particle numbers

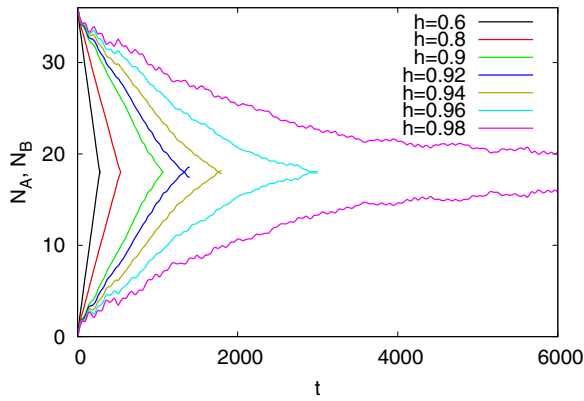


FIG. 2. Particle numbers of the two halves at different after-quench  $h$  fields, for the same system size  $L = 144$ , zero-temperature protocol. For oscillating parts, the curves are not shown, just the first crossing points.

will be equal. The slope of the initial decrease or increase is independent of the system size, and for  $t \ll L$  the increasing curves are identical.

In Fig. 2 the particle numbers are presented after different values of  $h$  and for a given system size ( $L = 144$ ). All of these quenches are in the extended phase, most of them close to the critical point. As the quench gets closer and closer to the critical point, the dynamics (slope of the curves) become slower and slower. The first crossing of the growing and decreasing particle numbers occurs later and later. I call the time of the first crossing the “crossing time.” One can obtain these crossing times using Fig. 2, and one can define a time scale using the crossing time.

The crossing times are presented in Fig. 1(b) as a function of the  $h$  parameter. The crossing time diverges approaching the critical point. The numerical fit shows  $0.98 \pm 0.03$  as the critical exponent; therefore the scaling of the first crossing time is likely to be

$$t_{\text{cross}} \sim \frac{1}{|1 - h|}. \quad (18)$$

In Fig. 3 the (log of the) growing particle number of the initially empty subsystem is shown as a function of  $\ln t$ . The particle number approximately grows as

$$N_B \sim t^{0.57}. \quad (19)$$

There are strong oscillations in the overall trend, which makes measurement of the exponent difficult. The exponent obtained here for the particle number is bigger than the exponents of the entanglement entropy and magnetization obtained in Ref. [31] for the case of global quenches.

In the context of front dynamics, it is usual to investigate the shape of the front. Here the local filling  $n_l = \langle c_l^\dagger(t)c_l(t) \rangle$  is investigated. However, the local value of this filling strongly depends on the on-site potential, and if one simply calculates it, no trend can be seen, only rapid oscillations. To define a meaningful front shape, one introduces a  $\varphi$  phase to the

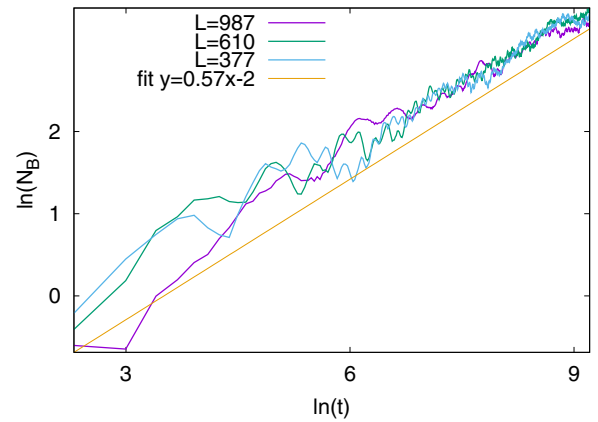


FIG. 3. Variation of the particle number (in the initially empty half) at a critical quench ( $h = 1$ ) for various system sizes, for the zero-temperature protocol. The straight line is a fit.

Hamiltonian

$$H = -\frac{1}{2} \sum_{l=1}^{L-1} c_l^\dagger c_{l+1} + c_{l+1}^\dagger c_l + h \sum_{l=1}^L \cos(2\pi\kappa l + \varphi) c_l^\dagger c_l \quad (20)$$

and averages over the  $\varphi$  phase. Different  $\varphi$  phases mean different relative positions of the lattice and the potential. So averaging over the phase is equivalent to averaging over the position where the boundary of the two initially distinct subsystems is located. In numerical calculations,  $10^4$  randomly chosen values of  $\varphi$  have been used (from the uniform distribution on  $[0, 2\pi]$ ).

The scaled front shapes are shown in Fig. 4. The front shapes can be scaled together, and the scaling exponent  $\alpha$  is different in the extended phase, at the critical point, and in the localized phase. The scaling function  $\Phi(x)$  (which is also different in the aforementioned three cases) can be defined as follows:

$$\Phi\left(\frac{j - L/2}{t^\alpha}\right) = n_j. \quad (21)$$

In the localized phase, the scaling is trivial; after a short initial evolution the front reaches a constant shape, i.e., it is “frozen in,” and this corresponds to  $\alpha_{\text{localized}} = 0$ . In the extended phase, the scaling exponent is found to be  $\alpha_{\text{extended}} = 1.0$ , which is identical to the scaling of the homogeneous XX chain front [4]. At the critical point, the best fit has been found at  $\alpha_{\text{critical}} = 0.55$ .

I investigated the mutual information in the zero-temperature quench between neighboring intervals around the initial connection point (one interval is from  $L/2 - l$  to  $L/2$ , and the other one is from  $L/2 + 1$  to  $L/2 + l$ ). The numerical results are shown in Figs. 4 and 5. In Fig. 5 the mutual information is shown as a function of the subsystem size  $\ln l$  at a given time  $t = 20$ . There is an initial growing region, and then a constant plateau starts. For the extended phase the mutual information for very small systems changes very slowly; for intermediate sizes there is a logarithmic growth, and then the plateau starts. Interestingly, at the critical point, there is no very slow initial region, and the mutual information

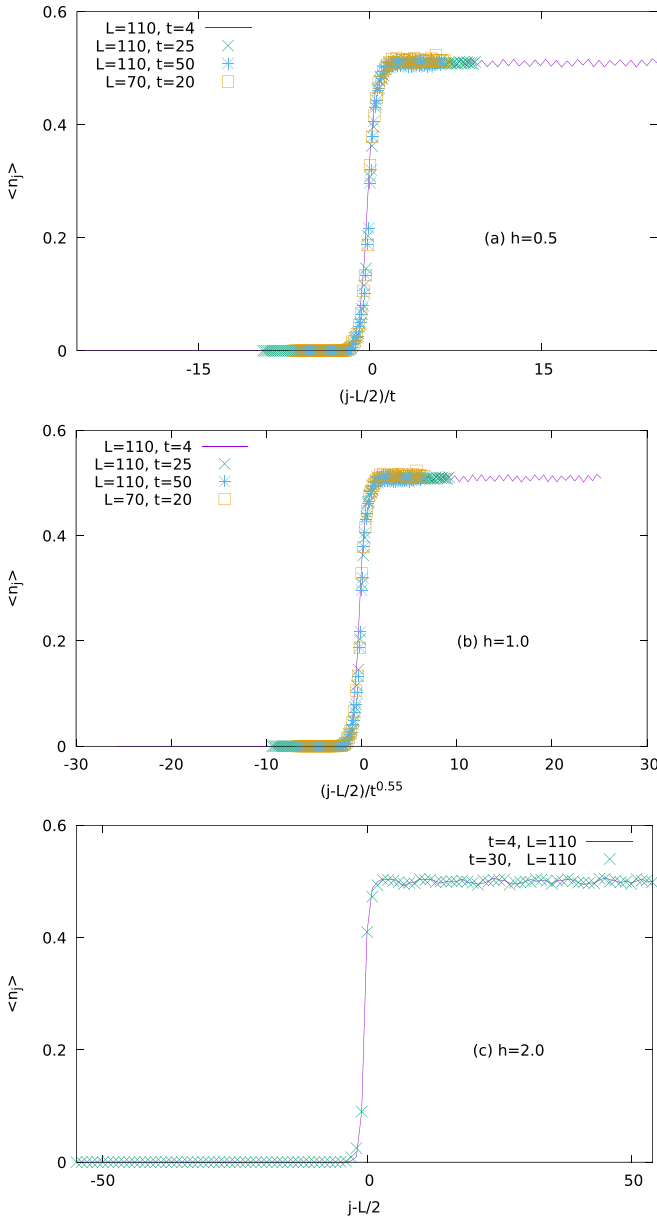


FIG. 4. Shape of the particle number front. The expectation value of the particle number  $n_j$  at position  $j$  in the extended phase (a), at the critical point (b), and in the localized phase (c), as a function of  $(j - L/2)/t^\alpha$  for various times and for  $L = 50, 70, 1110$ .

is proportional to the logarithm of the subsystem size from very small sizes. The numerical data are compatible with

$$I_{T=0, \text{extended}} \sim 1.1 \ln l, \quad (22)$$

$$I_{T=0, \text{critical}} \sim 0.51 \ln l. \quad (23)$$

Results regarding the time dependence of the mutual information for fixed system sizes are shown in Fig. 6. Here one finds that the mutual information is proportional to the logarithm of time, and the prefactors differ at the critical point and in the extended phase. In the localized phase the mutual

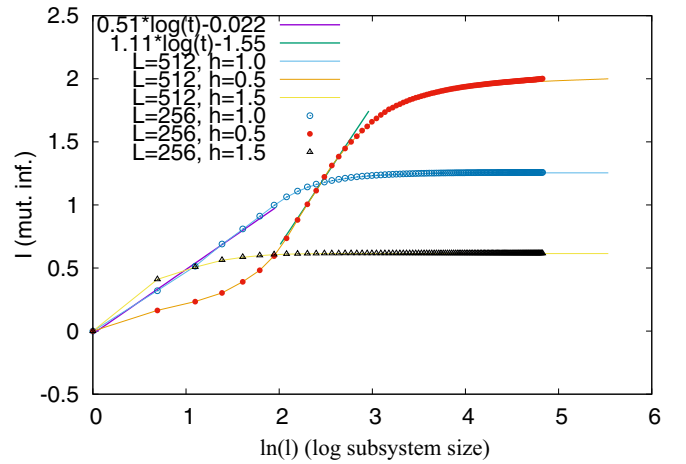


FIG. 5. Mutual information after the zero-temperature quench as a function of the logarithm of the subsystem size, at a given time  $t = 20$ . The straight lines show fits. Here, mut. inf., mutual information.

information converges to a constant value, independent of the subsystem and system sizes. The numerical data suggest

$$I_{T=0, \text{extended}} \sim 1.15 \ln t, \quad (24)$$

$$I_{T=0, \text{critical}} \sim 0.55 \ln t. \quad (25)$$

My results for the mutual information are in agreement with the results of Ref. [76], in which the entanglement entropy, not the mutual information, was calculated; however, for short times when the width of the front is smaller than the subsystem size  $l$  the time dependence of these two quantities has to be the same, and the numerical results are indeed very similar.

I calculated the mutual information in the finite-temperature quench. The temperatures were  $T_A = 0.5$  and  $T_B = 2.0$ .

In Figs. 7 and 8 the mutual information is shown after a finite-temperature quench averaged over 100 randomly chosen phases. There is an initial region (while the front size does not reach the system size) where the mutual information grows with the logarithm of time. This initial growth is found

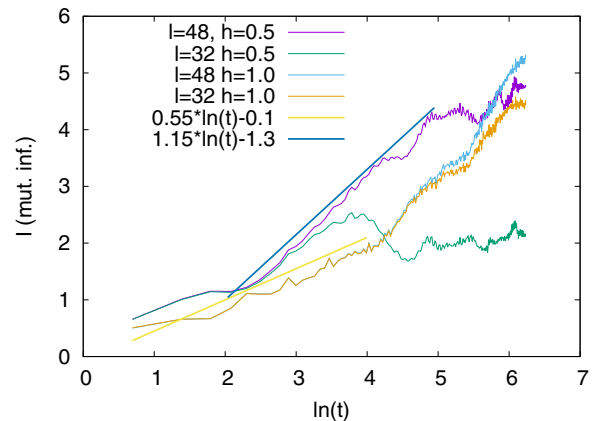


FIG. 6. Mutual information after the zero-temperature quench for a few fixed subsystem sizes, as a function of time.

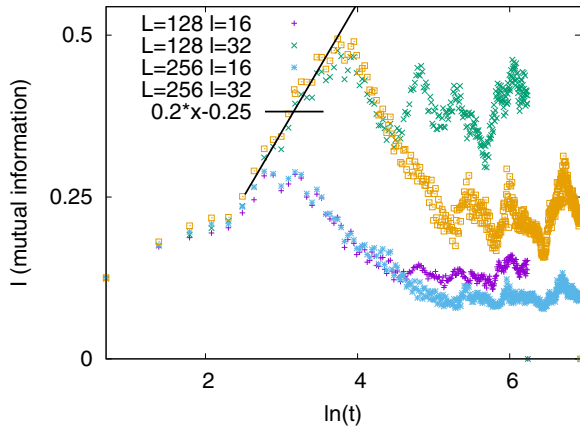


FIG. 7. Mutual information after finite-temperature quench for a few system and subsystem sizes, as a function of time, in the extended phase  $h = 0.5$ . The data are averaged over  $10^2$  randomly chosen phases.

to be

$$I_{T>0, \text{extended}} = 0.2 \ln(t) - 0.25. \quad (26)$$

At the critical point (see Fig. 8) the initial growth of the mutual information is

$$I_{T>0, \text{critical}} = 0.12 \ln(t) - 0.07. \quad (27)$$

In Fig. 9 the mutual information is shown as a function of the subsystem size. There is an initial slow region, a middle region where the variation of the mutual information is proportional to the logarithm of the subsystem size, and, for big subsystem sizes, a constant value at which the mutual information converges. The middle logarithmic part is found to be

$$I_{T>0, \text{extended}} = 0.48 \ln l - 1.2, \quad (28)$$

$$I_{T>0, \text{critical}} = 0.21 \ln l - 0.14. \quad (29)$$

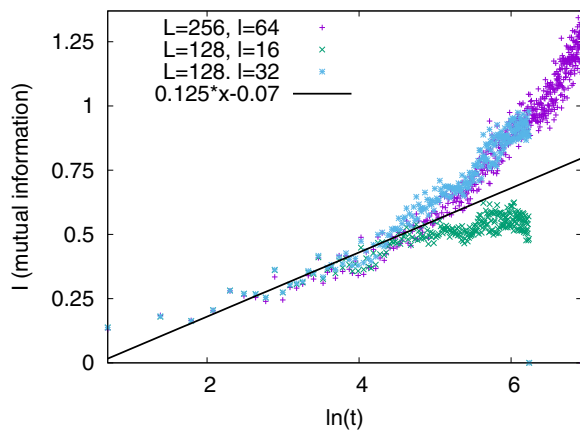


FIG. 8. Mutual information after finite-temperature quench for a few system and subsystem sizes, as a function of time, at the critical point  $h = 1.00$ . The data are averaged over  $10^2$  randomly chosen phases.

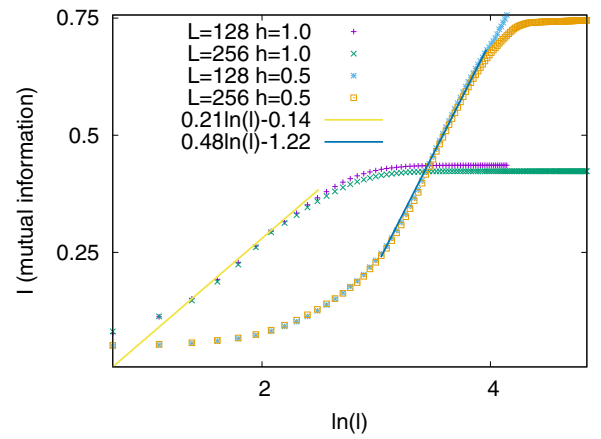


FIG. 9. Mutual information after a finite-temperature quench at a fixed time  $t = 60$ , as a function of the subsystem sizes.

## V. CONCLUSIONS

Here the front dynamics of a noninteracting model with a localization transition have been investigated. In the extended phase the dynamics are qualitatively similar to the homogeneous XX front dynamics [7]. However, when approaching the critical point, the time scale of the dynamics (defined by the crossing time in this paper) diverges with an exponent of 1, and at the critical point, slower, diffusive dynamics occur. In the case of the zero-temperature quench, where the initial difference is the particle number, the front shapes can be scaled together. For the localized phase the scaling is trivial, and for the extended phase, the scaling is equivalent to the scaling of the homogeneous system. At the critical point, the scaling includes a power law  $t^{0.5}$ . This exponent is close to the literature value of the wave packet spreading exponent of the Harper model [64,67], which is known to be 0.477. There is a simple reason behind this phenomenon: If half of a system is filled and the other half is empty, one can perform a particle-hole transformation on the filled half of the system, and in the resulting effective system, the problem is equivalent to a local quench. However, the initial state used here is not fully empty or fully filled; rather, one half is initially empty, and the other half is initially half filled: This may cause the difference between the wave packet scaling exponent known from the literature and the front shape scaling exponent measured here. A similar simple connection between the finite-temperature initial state and the local quenches does not exist. The scaling of the mutual information with the subsystem size and time is found to be logarithmic both in the extended phase and at the critical point. The prefactors of the time and subsystem size dependence agree up to the precision of this work in the zero-temperature quench; however, in the finite-temperature quench they are significantly different.

This is a major difference compared with the homogeneous XX chain, where the prefactor of the logarithmic scaling of the mutual information is the same for the time and space dependence.

The prefactors of the mutual information at the critical point are generally smaller than those in the extended phase; this phenomenon is similar to the entanglement scaling found in Ref. [67].

Further generalizations of the present work may include numerical studies of the dependence of the dynamics on the irrational potential or numerical studies in a generalization of the present model where the quasiperiodic potential is  $\cos(2\pi\kappa l^\alpha)$ , in which the details of the transition depend on the  $\alpha$  exponent [77].

### ACKNOWLEDGMENTS

The author thanks F. Iglói, R. Juhász, and Z. Zimborás for useful discussions. This work was supported by the National Research, Development and Innovation Office (NKFIH) under Grant No. K128989. This work was supported by the National Quantum Information Laboratory of Hungary.

### APPENDIX: TIME EVOLUTION

I use the Heisenberg picture. It is possible to treat the two protocols in a unified way. The only difference is the calculation of the initial correlations. The initial state is characterized by its two-point correlation function,

$$g_{l,m} = \langle c_l^\dagger c_m \rangle. \quad (\text{A1})$$

In the case of the first protocol (particle number quench), to calculate this correlation function, I used a modified initial Hamiltonian. I added a big (100) local potential to one part (the  $A$  part) of the Hamiltonian and diagonalized this modified Hamiltonian. With this high potential, the  $A$  part is practically empty.

$$H = -\frac{1}{2} \sum_{l=1}^{L-1} c_l^\dagger c_{l+1} + c_{l+1}^\dagger c_l + h \sum_{l=1}^L \cos(2\pi\kappa l) c_l^\dagger c_l + 100 \sum_{l=1}^{L/2} c_l^\dagger c_l. \quad (\text{A2})$$

One diagonalizes the modified Hamiltonian with a canonical transformation

$$\eta_k = \sum_{l=1}^L u_{k,l}^{(0)} c_l, \quad (\text{A3})$$

$$H = \sum_{k=1}^L \epsilon_k^{(0)} \eta_k^\dagger \eta_k, \quad (\text{A4})$$

and the initial correlations are given by

$$g_{l,m} = \sum_{k, \epsilon_k < 0} u_{k,l} u_{k,m}. \quad (\text{A5})$$

For the second protocol (temperature quench), one diagonalizes  $H_A$  and  $H_B$  separately, the correlations in  $A$  ( $B$ ) are determined by  $H_A$  ( $H_B$ ), and the correlations between the two subsystems are zero.

$$H_A = -\frac{1}{2} \sum_{l=1}^{L/2-1} c_l^\dagger c_{l+1} + c_{l+1}^\dagger c_l + h \sum_{l=1}^{L/2} \cos(2\pi\kappa l) c_l^\dagger c_l, \quad (\text{A6})$$

$$H_B = -\frac{1}{2} \sum_{l=L/2}^{L-1} c_l^\dagger c_{l+1} + c_{l+1}^\dagger c_l + h \sum_{l=L/2}^L \cos(2\pi\kappa l) c_l^\dagger c_l, \quad (\text{A7})$$

$$\eta_k^A = \sum_{l=1}^{L/2} u_{k,l}^{A,(0)} c_l, \quad (\text{A8})$$

$$H = \sum_{k=1}^{L/2} \epsilon_k^{A,(0)} \eta_k^\dagger \eta_k, \quad (\text{A9})$$

$$\eta_k^B = \sum_{l=L/2}^L u_{k,l}^{B,(0)} c_l, \quad (\text{A10})$$

$$H = \sum_{k=L/2}^L \epsilon_k^{B,(0)} \eta_k^\dagger \eta_k. \quad (\text{A11})$$

The correlation function is given by

$$g_{l,m} = \begin{cases} \sum_k u_{k,l}^{A,(0)} u_{k,m}^{A,(0)} n(\epsilon_k, T_A) & \text{if } l, m \in A \\ \sum_k u_{k,l}^{B,(0)} u_{k,m}^{B,(0)} n(\epsilon_k, T_B) & \text{if } l, m \in B \\ 0 & \text{if } l \in A \text{ and } m \in B \\ 0 & \text{if } l \in B \text{ and } m \in A, \end{cases} \quad (\text{A12})$$

where  $n(\epsilon, T) = 1/(\exp[\epsilon/T] + 1)$  is the Fermi function.

For  $t > 0$ , one diagonalizes the after-quench Hamiltonian

$$v_k = \sum_{l=1}^L u_{k,l} c_l, \quad (\text{A13})$$

$$H = \sum_{k=1}^L \epsilon_k v_k^\dagger v_k. \quad (\text{A14})$$

The time evolution of the  $v$  operators in the Heisenberg picture is  $v(t) = e^{-i\epsilon_k t} v(0)$ ,  $v^\dagger(t) = e^{-i\epsilon_k t} v^\dagger(0)$ .

The time evolution of the  $c_l$  operators is

$$c_l(t) = \sum_{k=1}^L u_{k,l} e^{-i\epsilon_k t} v_k(0) \quad (\text{A15})$$

$$= \sum_{l=1}^L \sum_{m=1}^L \sum_{k=1}^L u_{k,l} e^{-i\epsilon_k t} u_{k,m} c_m(0) \quad (\text{A16})$$

$$= \sum_{l=1}^L \sum_{m=1}^L f(m, l, t) c_m(0), \quad (\text{A17})$$

$$f(m, l, t) = \sum_{k=1}^L u_{k,l} e^{-i\epsilon_k t} u_{k,m}. \quad (\text{A18})$$

The time evolution of the particle number operators  $\hat{N}_A$ ,  $\hat{N}_B$  and the local Hamiltonians  $H_A$ ,  $H_B$  can be written as bilinear expressions using Eq. (A18). The expectation values are

$$\langle \hat{N}_A \rangle = \sum_{l=1}^{L/2} \sum_{n=1}^L \sum_{m=1}^L f^*(n, l, t) f(m, l, t) g_{n,m}, \quad (\text{A19})$$

$$\langle \hat{N}_B \rangle = \sum_{l=L/2}^L \sum_{n=1}^L \sum_{m=1}^L f^*(n, l, t) f(m, l, t) g_{n,m}, \quad (\text{A20})$$

$$\begin{aligned}
\langle H_A \rangle &= \sum_{l=1}^{L/2} \sum_{n=1}^L \sum_{m=1}^{L/2} f^*(n, l, t) f(m, l, t) g_{n,m} h \cos(2\pi \kappa l) \\
&+ \sum_{n=1}^L \sum_{m=1}^L \frac{1}{2} (f^*(n, l+1, t) f(m, l, t) \\
&+ f(n, l+1, t) f^*(m, l, t)) g_{n,m}, \tag{A21}
\end{aligned}$$

$$\begin{aligned}
\langle H_B \rangle &= \sum_{l=L/2}^L \sum_{n=1}^L \sum_{m=1}^L f^*(n, l, t) f(m, l, t) g_{n,m} h \cos(2\pi \kappa l) \\
&+ \sum_{n=1}^L \sum_{m=1}^L \frac{1}{2} (f^*(n, l+1, t) f(m, l, t) \\
&+ f(n, l+1, t) f^*(m, l, t)) g_{n,m}. \tag{A22}
\end{aligned}$$

- 
- [1] T. Antal, Z. Rácz, A. Rákos, and G. M. Schütz, *Phys. Rev. E* **59**, 4912 (1999).
- [2] Y. Ogata, *Phys. Rev. E* **66**, 066123 (2002).
- [3] D. Karevski, *Eur. Phys. J. B* **27**, 147 (2002).
- [4] V. Hunyadi, Z. Rácz, and L. Sasvári, *Phys. Rev. E* **69**, 066103 (2004).
- [5] T. Antal, Z. Rácz, and L. Sasvári, *Phys. Rev. Lett.* **78**, 167 (1997).
- [6] T. Antal, Z. Rácz, A. Rákos, and G. M. Schütz, *Phys. Rev. E* **57**, 5184 (1998).
- [7] V. Eisler and Z. Zimboras, *Phys. Rev. A* **89**, 032321 (2014).
- [8] V. Eisler and Z. Rácz, *Phys. Rev. Lett.* **110**, 060602 (2013).
- [9] T. Platini and D. Karevski, *J. Phys. A: Math. Theor.* **40**, 1711 (2007).
- [10] H. Moriya, R. Nagao, and T. Sasamoto, *J. Stat. Mech.* (2019) 063105.
- [11] F. Rottoli, S. Scopa, and P. Calabrese, *J. Stat. Mech.* (2022) 063103.
- [12] M. Kormos, *SciPost Phys.* **3**, 020 (2017).
- [13] G. Peretto and A. Gambassi, *Phys. Rev. E* **96**, 012138 (2017).
- [14] S. Bhattacharyya and S. Dasgupta, *Eur. Phys. J. B* **90**, 140 (2017).
- [15] V. Eisler, F. Maislinger, and H. Gerd Evertz, *SciPost Phys.* **1**, 014 (2016).
- [16] M. Kormos and Z. Zimborás, *J. Phys. A: Math. Theor.* **50**, 264005 (2017).
- [17] T. Platini and D. Karevski, *J. Phys.: Conf. Ser.* **40**, 93 (2006).
- [18] T. Platini and D. Karevski, *Eur. Phys. J. B* **48**, 225 (2005).
- [19] V. Eisler and F. Maislinger, *SciPost Phys.* **8**, 037 (2020).
- [20] S. Scopa, P. Calabrese, and J. Dubail, *SciPost Phys.* **12**, 207 (2022).
- [21] J. Lopez-Piqueres, B. Ware, S. Gopalakrishnan, and R. Vasseur, *Phys. Rev. B* **104**, 104307 (2021).
- [22] M. Collura, A. De Luca, P. Calabrese, and J. Dubail, *Phys. Rev. B* **102**, 180409(R) (2020).
- [23] V. B. Bulchandani and C. Karrasch, *Phys. Rev. B* **99**, 121410(R) (2019).
- [24] V. Eisler and D. Bauernfeind, *Phys. Rev. B* **96**, 174301 (2017).
- [25] T. Sabetta and G. Misguich, *Phys. Rev. B* **88**, 245114 (2013).
- [26] M. Einhellinger, A. Cojuhovski, and E. Jeckelmann, *Phys. Rev. B* **85**, 235141 (2012).
- [27] J. Lancaster and A. Mitra, *Phys. Rev. E* **81**, 061134 (2010).
- [28] S. Langer, F. Heidrich-Meisner, J. Gemmer, I. P. McCulloch, and U. Schollwöck, *Phys. Rev. B* **79**, 214409 (2009).
- [29] T. Antal, P. L. Krapivsky, and A. Rákos, *Phys. Rev. E* **78**, 061115 (2008).
- [30] D. Gobert, C. Kollath, U. Schollwöck, and G. Schütz, *Phys. Rev. E* **71**, 036102 (2005).
- [31] G. Roósz, U. Divakaran, H. Rieger, and F. Iglói, *Phys. Rev. B* **90**, 184202 (2014).
- [32] E. Lieb, T. Schultz, and D. Mattis, *Ann. Phys. (NY)* **16**, 407 (1961).
- [33] P. Jordan and E. Wigner, *Z. Phys.* **47**, 631 (1928).
- [34] V. Eisler and Z. Zimboras, *New J. Phys.* **16**, 123020 (2014).
- [35] D. X. Horváth, S. Sotiriadis, M. Kormos, and G. Takács, *SciPost Phys.* **12**, 144 (2022).
- [36] P. Calabrese and J. Cardy, *J. Stat. Mech.* (2007) P06008.
- [37] P. Calabrese and J. Cardy, *J. Stat. Mech.* (2005) P04010.
- [38] F. Iglói and H. Rieger, *Phys. Rev. Lett.* **106**, 035701 (2011).
- [39] H. Rieger and F. Iglói, *Phys. Rev. B* **84**, 165117 (2011).
- [40] V. Alba, B. Bertini, and M. Fagotti, *SciPost Phys.* **7**, 005 (2019).
- [41] B. Bertini, M. Fagotti, L. Piroli, and P. Calabrese, *J. Phys. A: Math. Theor.* **51**, 39LT01 (2018).
- [42] O. A. Castro-Alvaredo, B. Doyon, and T. Yoshimura, *Phys. Rev. X* **6**, 041065 (2016).
- [43] P. Ruggiero, P. Calabrese, B. Doyon, and J. Dubail, *Phys. Rev. Lett.* **124**, 140603 (2020).
- [44] B. Doyon, *SciPost Phys. Lect. Notes* **18** (2020).
- [45] G. Misguich, N. Pavloff, and V. Pasquier, *SciPost Phys.* **7**, 025 (2019).
- [46] V. Alba, B. Bertini, M. Fagotti, L. Piroli, and P. Ruggiero, *J. Stat. Mech.* (2021) 114004.
- [47] I. Bouchoule and J. Dubail, *J. Stat. Mech.* (2022) 014003.
- [48] M. Fagotti, *Phys. Rev. B* **96**, 220302(R) (2017).
- [49] P. Ruggiero, P. Calabrese, B. Doyon, and J. Dubail, *J. Phys. A: Math. Theor.* **55**, 024003 (2022).
- [50] A. Bastianello, V. Alba, and J.-S. Caux, *Phys. Rev. Lett.* **123**, 130602 (2019).
- [51] V. B. Bulchandani, R. Vasseur, C. Karrasch, and J. E. Moore, *Phys. Rev. Lett.* **119**, 220604 (2017).
- [52] B. Doyon, T. Yoshimura, and J.-S. Caux, *Phys. Rev. Lett.* **120**, 045301 (2018).
- [53] M. Schemmer, I. Bouchoule, B. Doyon, and J. Dubail, *Phys. Rev. Lett.* **122**, 090601 (2019).
- [54] N. Malvania, Y. Zhang, Y. Le, J. Dubail, M. Rigol, and D. S. Weiss, *Science* **373**, 1129 (2021).
- [55] F. Iglói, Z. Szatmári, and Y. C. Lin, *Phys. Rev. B* **85**, 094417 (2012).
- [56] F. Iglói, G. Roósz, and Y. C. Lin, *New J. Phys.* **15**, 023036 (2013).
- [57] G. Roósz, Y. C. Lin, and F. Iglói, *New J. Phys.* **19**, 023055 (2017).
- [58] S. Aubry and G. André, *Ann. Isr. Phys. Soc.* **3**, 133 (1980).
- [59] D. J. Thouless, *Phys. Rev. B* **28**, 4272 (1983).
- [60] P. G. Harper, *Proc. Phys. Soc. A* **68**, 874 (1955).
- [61] F. Evers and A. D. Mirlin, *Rev. Mod. Phys.* **80**, 1355 (2008).

- [62] T. Cookmeyer, J. Motruk, and J. E. Moore, *Phys. Rev. B* **101**, 174203 (2020).
- [63] A. Sinha, M. M. Rams, and J. Dziarmaga, *Phys. Rev. B* **99**, 094203 (2019).
- [64] M. Wilkinson and E. J. Austin, *Phys. Rev. B* **50**, 1420 (1994).
- [65] S. N. Evangelou and J.-L. Pichard, *Phys. Rev. Lett.* **84**, 1643 (2000).
- [66] A. P. Siebesma and L. Pietronero, *Europhys. Lett.* **4**, 597 (1987).
- [67] G. Roósz, Z. Zimborás, and R. Juhász, *Phys. Rev. B* **102**, 064204 (2020).
- [68] N. Roy and A. Sharma, *Phys. Rev. B* **100**, 195143 (2019).
- [69] J. Hauschild, F. Pollmann, and F. Heidrich-Meisner, *Phys. Rev. A* **92**, 053629 (2015).
- [70] J. P. Ronzheimer, M. Schreiber, S. Braun, S. S. Hodgman, S. Langer, I. P. McCulloch, F. Heidrich-Meisner, I. Bloch, and U. Schneider, *Phys. Rev. Lett.* **110**, 205301 (2013).
- [71] M. Modugno, *New J. Phys.* **11**, 033023 (2009).
- [72] B. Deissler, E. Lucioni, M. Modugno, G. Roati, L. Tanzi, M. Zaccanti, M. Inguscio, and G. Modugno, *New J. Phys.* **13**, 023020 (2011).
- [73] J.-y. Choi, S. Hild, J. Zeiher, P. Schauß, A. Rubio-Abadal, T. Yefsah, V. Khemani, D. A. Huse, I. Bloch, and C. Gross, *Science* **352**, 1547 (2016).
- [74] C. H. Bennett, H. J. Bernstein, S. Popescu, and B. Schumacher, *Phys. Rev. A* **53**, 2046 (1996).
- [75] M. A. Nielsen and I. L. Chuang, *Quantum Computation and Quantum Information* (Cambridge University Press, Cambridge, UK, 2000).
- [76] A. Ahmed, N. Roy, and A. Sharma, *Phys. Rev. B* **104**, 155137 (2021).
- [77] I. Varga, J. Pipek, and B. Vasvári, *Phys. Rev. B* **46**, 4978 (1992).